Hopf Bifurcation and Chaos in a Free-Running Current-Controlled Ćuk Switching Regulator

C. K. Tse, *Senior Member, IEEE*, Y. M. Lai, *Member, IEEE*, and H. H. C. Iu, *Student Member, IEEE*

***Abstract*—An autonomous free-running Ćuk converter is studied in this paper. Analysis of the describing nonlinear state equations shows that the system loses stability via a supercritical Hopf bifurcation. The boundary of stability is derived and local trajectories of motion studied. Cycle-by-cycle simulations of the actual system reveal the typical bifurcation from a stable equilibrium state to chaos, via limit cycles, and quasi-periodic orbits. Experimental measurements confirm the bifurcation scenarios. The occurrence of such kinds of bifurcation in autonomous dc/dc converters has been rarely known in power electronics.**

***Index Terms*—Bifurcation, chaos, Ćuk converter, dc/dc converter, power electronics.**

I. Introduction

POWER electronics is a field rich in nonlinear dynamics [1], and engineers who work in this field are frequent "chaos observers" whether they know it or not. In fact, during the early development and testing stages of power electronics systems, a multitude of nonlinear phemenona, such as subharmonics, quasi-periodicity and chaos, are almost invariably encountered. Because power electronics engineers are primarily concerned with only the regular periodic (fixed point) operation, they tend to avoid any "strange" operation by adjusting components or parameters that they believe are causing problems to their systems. Very often such adjustment processes are done in a trial-and-error manner. However, to achieve more reliable designs, we need a better understanding of the circuit operation under all possible practical conditions. Moreover, we may open up new possibilities in operating power electronics systems if enough understanding is gained of the many unused operating regimes.

Self-oscillating or free-running current-controlled switching converters are often used in low-cost switching power supplies, since they require no external clocks and their constructions are relatively simple. In contrast to their nonautonomous counterparts for which chaos is observed even for the simplest first-order discontinuous-mode converters [2], [3], free-running converters of order below three cannot exhibit chaos. The essential feature of an autonomous switching converter is the absence of any external driving signal, which is mandatory in the nonautonomous case for periodic switching of the power switch. Until now, much has been reported on the bifurcation and chaotic behavior of nonautonomous switching converters [2]–[8], while very little work has been performed in identifying bifurcation and chaos in autonomous switching converters. In this paper we study the dynamics of the Ćuk converter which is widely used in power electronics. Being of fourth-order, the Ćuk converter can operate chaotically in free-running (autonomous) mode. We will report in this paper the bifurcation behavior of a free-running current-controlled Ćuk converter. In particular, our study will cover the following aspects: 1) derivation of describing state equation; 2) study of stability of the equilibrium state and identification of Hopf bifurcation based on the describing state equation; 3) computer simulations of the circuits revealing the bifurcation from stable equilibrium state (fixed point), through limit cycles and quasi-periodic orbits, and eventually to chaos; and 4) experimental verification of the bifurcation scenario.

Manuscript received March 11, 1999; revised August 19, 1999. This work was supported by the Hong Kong Research Grants Council under a competitive earmarked research Grant PolyU109/96E. This paper was recommended by Associate Editor C. W. Wu.

The authors are with the Department of Electronic and Information Engineering, Hong Kong Polytechnic University, Kowloon, Hong Kong, China. (e-mail: cktse@eie.polyu.edu.hk).

Publisher Item Identifier S 1057-7122(00)02915-9.

II. System Description

Specifically, the system under study consists of a Ćuk converter whose operation is based on a free-running hysteretic current-mode control. In actual implementation the switch is turned on and off, in a hysteretic fashion, when the sum of the inductor currents falls below or rises above a certain preset hysteretic band [9], [10]. The average value and width of this preset band are adjusted by a feedback Schmitt trigger circuit. Also, the output voltage is fed back to set the average value of the hysteretic band, forcing the control variable to be related by the following control equation:

$$i_1 + i_2 = g(v_1) \tag{1}$$

where

i_1 and i_2	inductor currents;
v_1	output voltage;
$g(.)$	control function.

For example, a simple proportional control takes the form of

$$\Delta(i_1 + i_2) = -\mu \Delta v_1 \tag{2}$$

where μ is the gain factor. This equation has the following equivalent form, assuming regulated output:

$$i_1 + i_2 = K - \mu v_1 \tag{3}$$

where K and μ are the control parameters. Fig. 1 shows a simplified schematic of the system.

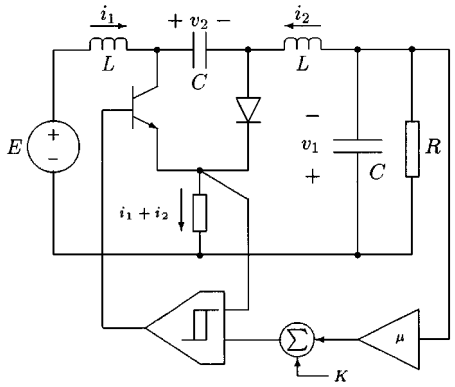

Fig. 1. Ćuk converter under hysteretic current-mode control.

A. Derivation of Autonomous State Equations

The system can be represented by the following state-space equations where $s = 1$ when the switch is turned on, and $s = 0$ when the switch is off:

$$\begin{cases} \dfrac{di_1}{dt} = -\dfrac{(1-s)v_2}{L} + \dfrac{E}{L} \\ \dfrac{di_2}{dt} = \dfrac{v_2 s}{L} - \dfrac{v_1}{L} \\ \dfrac{dv_1}{dt} = \dfrac{i_2}{C} - \dfrac{v_1}{CR} \\ \dfrac{dv_2}{dt} = \dfrac{(1-s)i_1}{C} - \dfrac{i_2 s}{C}. \end{cases} \tag{4}$$

The state-space averaged model has the same form as above, with s replaced by the duty cycle δ which is the fraction of the switching period for which the switch is turned on.

Since $i_1 + i_2$ is related to v_1 by a linear algebraic equation, the system reduces its order by one. Specifically, when (3) is taken into account, the system can be reduced to the following third-order system:

$$\begin{cases} \dfrac{di_2}{dt} = \dfrac{v_2\delta}{L} - \dfrac{v_1}{L} \\ \dfrac{dv_1}{dt} = \dfrac{i_2}{C} - \dfrac{v_1}{CR} \\ \dfrac{dv_2}{dt} = \dfrac{(1-\delta)(K-\mu v_1)}{C} - \dfrac{i_2}{C} \end{cases} \tag{5}$$

where δ is the duty cycle. Also, from (3), $d(i_1 + i_2)/dt = -\mu\, dv_1/dt$. Substitution of the involving derivatives gives

$$\delta = \frac{1}{2} - \frac{\dfrac{\mu L}{C} i_2 - \left(1 + \dfrac{\mu L}{CR}\right) v_1 + E}{2v_2} \tag{6}$$

which must satisfy $0 < \delta < 1$. Finally, putting (6) into (5) results in the following state equations that describe the dynamics of the autonomous system:

$$\begin{cases} \dfrac{di_2}{dt} = -\dfrac{\mu i_2}{2C} - \left(1 - \dfrac{\mu L}{CR}\right)\dfrac{v_1}{2L} + \dfrac{v_2}{2L} - \dfrac{E}{2L} \\ \dfrac{dv_1}{dt} = \dfrac{i_2}{C} - \dfrac{v_1}{CR} \\ \dfrac{dv_2}{dt} = -\dfrac{i_2}{C} + \left(\dfrac{K - \mu v_1}{2C}\right) \\ \qquad \cdot \left(1 + \dfrac{\frac{\mu L}{C} i_2 - \left(1 + \frac{\mu L}{CR}\right) v_1 + E}{v_2}\right). \end{cases} \tag{7}$$

Note that this representation is valid only if $0 < \delta < 1$. Such a condition is satisfied when the system is operating in stable equilibrium state, corresponding to a fixed point in the above averaged model.

Remarks: It should be noted that averaged models have limited validity for nonlinear analysis. Specifically, the averaged model, as derived above, is valid when the system remains in continuous mode and the switching frequency is relatively high. Thus, we may use such a model only to study the behavior of the system up to the point of losing stability. Nonetheless, as we will see, the averaged model gives useful clues to the way the system loses stability, although it stops short of predicting the behavior beyond the bifurcation point.

B. Equilibrium Point Calculation

To find the equilibrium point, we set all the time-derivatives to zero and solve for i_2, v_1, and v_2. This gives

$$\begin{cases} I_2 = -\dfrac{E(1+\mu R)}{2R} \pm \dfrac{E}{2R}\sqrt{(1+\mu R)^2 + \dfrac{4KR}{E}} \\ V_1 = -\dfrac{E(1+\mu R)}{2} \pm \dfrac{E}{2}\sqrt{(1+\mu R)^2 + \dfrac{4KR}{E}} \\ V_2 = \dfrac{E(1-\mu R)}{2} \pm \dfrac{E}{2}\sqrt{(1+\mu R)^2 + \dfrac{4KR}{E}} \end{cases} . \tag{8}$$

Note that the choice of the control parameters K and μ will set the steady-state output voltage level, provided the system is stable. The stability of the system is yet to be studied for different sets of parameters. Furthermore, assuming the existence of a stable steady state, the value of the duty cycle can be found by putting $V_1 = I_2 R$ in (6)

$$\delta|_{\text{steady-state}} = \frac{1}{2} - \frac{E - V_1}{2V_2}. \tag{9}$$

Also, since $V_2 = V_1 + E$, we can write

$$\delta|_{\text{steady-state}} = \frac{V_1}{E + V_1}. \tag{10}$$

Since $E > 0$ and $\delta \in [0, 1]$, $V_1 < 0$ is not possible. Thus, we have $V_1 > 0$ and the only equilibrium point is given by

$$\begin{cases} V_1 = I_2 R = -\dfrac{E(1+\mu R)}{2} + \dfrac{E}{2}\sqrt{(1+\mu R)^2 + \dfrac{4KR}{E}} \\ V_2 = \dfrac{E(1-\mu R)}{2} + \dfrac{E}{2}\sqrt{(1+\mu R)^2 + \dfrac{4KR}{E}}. \end{cases} \tag{11}$$

C. Dimensionless Equations

The afore-derived state equations can be put in a dimensionless form. Define the dimensionless state variables as follows:

$$x_1 = \frac{Ri_2}{E}, \qquad x_2 = \frac{v_1}{E}, \qquad x_3 = \frac{v_2}{E}. \tag{12}$$

Also define the dimensionless time and parameters as follows:

$$\tau = \frac{Rt}{2L}, \qquad \xi = \frac{L/R}{CR}, \qquad \kappa_1 = \mu R, \qquad \kappa_o = \frac{KR}{E}. \tag{13}$$

Direct substitution of these new dimensionless variables, time, and parameters in the autonomous equations of (7) yields the following dimensionless autonomous equations:

$$\begin{cases} \dfrac{dx_1}{d\tau} = -\xi\kappa_1 x_1 - (1-\kappa_1\xi)x_2 + x_3 - 1 \\ \dfrac{dx_2}{d\tau} = 2\xi(x_1 - x_2) \\ \dfrac{dx_3}{d\tau} = -2\xi x_1 + \xi(\kappa_o - \kappa_1 x_2) \\ \qquad\qquad \cdot\left(1 + \dfrac{\kappa_1\xi x_1 - (1+\kappa_1\xi)x_2 + 1}{x_3}\right). \end{cases} \tag{14}$$

To complete the model, saturation must be included. Now, δ may be written as

$$\delta = 0.5 - \frac{\kappa_1\xi x_1 - (1+\kappa_1\xi)x_2 + 1}{2x_3}. \tag{15}$$

The condition for saturation is

$$\delta > 1 \Leftrightarrow \kappa_1\xi x_1 - (1+\kappa_1\xi)x_2 + x_3 + 1 < 0 \tag{16}$$

or

$$\delta < 0 \Leftrightarrow \kappa_1\xi x_1 - (1+\kappa_1\xi)x_2 - x_3 + 1 > 0. \tag{17}$$

By putting $\delta = 1$ or 0 in (5) and performing dimensionless substitution, the state equations for saturation are

$$\begin{cases} \dfrac{dx_1}{d\tau} = 2(x_3 - x_2) \\ \dfrac{dx_2}{d\tau} = 2\xi(x_1 - x_2), \qquad \text{for } \delta > 1 \\ \dfrac{dx_3}{d\tau} = -2\xi x_1 \end{cases} \tag{18}$$

and

$$\begin{cases} \dfrac{dx_1}{d\tau} = -2x_2 \\ \dfrac{dx_2}{d\tau} = 2\xi(x_1 - x_2) \qquad , \qquad \text{for } \delta < 0. \\ \dfrac{dx_3}{d\tau} = -2\xi x_1 + 2\xi(\kappa_0 - \kappa_1 x_2) \end{cases} \tag{19}$$

The equilibrium point can be calculated by putting $dx_1/d\tau = dx_2/d\tau = dx_3/d\tau = 0$ in (14) and considering the restricted sign of X_2. This gives

$$X = \begin{bmatrix} X_1 \\ X_2 \\ X_3 \end{bmatrix} = \begin{bmatrix} X_s \\ X_s \\ X_s + 1 \end{bmatrix} \tag{20}$$

where

$$X_s = \frac{-(1+\kappa_1) + \sqrt{(1+\kappa_1)^2 + 4\kappa_o}}{2}. \tag{21}$$

III. Stability of Equilibrium Point and Hopf Bifurcation

The Jacobian matrix, $J(X)$, for the dimensionless system evaluated at the equilibrium point is given by

$$J(X) = \begin{bmatrix} -\kappa_1\xi & -(1-\kappa_1\xi) & 1 \\ 2\xi & -2\xi & 0 \\ J_{31} & J_{32} & J_{33} \end{bmatrix}$$

where

$$J_{31} = -2\xi + \frac{\kappa_1\xi^2(\kappa_o - \kappa_1 X_s)}{1+X_s} \tag{22}$$

$$J_{32} = \frac{-2\kappa_1\xi - \xi(1+\kappa_1\xi)(\kappa_o - \kappa_1 X_s)}{1+X_s} \tag{23}$$

$$J_{33} = \frac{\xi(\kappa_o - \kappa_1 X_s)(X_s - 1)}{(1+X_s)^2}. \tag{24}$$

From (21), $X_s(X_s + 1) = \kappa_o\kappa_1 X_s$. The Jacobian matrix can hence be simplified to (25), as shown at the bottom of the page.

$$J(X) = \begin{bmatrix} -\kappa_1\xi & -(1-\kappa_1\xi) & 1 \\ 2\xi & -2\xi & 0 \\ -2\xi + \kappa_1\xi^2 X_s & \dfrac{-2\kappa_1\xi}{1+X_s} - \xi(1+\kappa_1\xi)X_s & \dfrac{-\xi X_s(1-X_s)}{1+X_s} \end{bmatrix} \tag{25}$$

TABLE I
EIGENVALUES AT $\xi = 0.0136$ SHOWING DEPENDENCE ON κ_0

	$\kappa_1 = 1$	Remarks
$\kappa_0 = 1$	$-0.0078725 \pm j0.232363$, -0.0274423	Stable equilibrium point
$\kappa_0 = 3$	$-0.00666899 \pm j0.232102$, -0.0275472	Stable equilibrium point
$\kappa_0 = 5$	$-0.00482465 \pm j0.231866$, -0.0275798	Stable equilibrium point
$\kappa_0 = 7$	$-0.0029592 \pm j0.231535$, -0.0276402	Stable equilibrium point
$\kappa_0 = 9$	$-0.0011668 \pm j0.231428$, -0.0276955	Stable equilibrium point
$\kappa_0 = 11$	$0.000538546 \pm j0.231217$, -0.0277466	Unstable equilibrium point

We shall attempt to study the stability of the equilibrium point and the trajectory around the equilibrium point by deriving the eigenvalues of the system at the equilibrium point. The usual procedure is to solve the following equation for λ:

$$\det[\lambda \boldsymbol{I} - J(X)] = 0. \tag{26}$$

Upon expanding, we get

$$\lambda^3 + \frac{\xi[(\kappa_1+2)+(\kappa_1+3)X_s - X_s^2]}{1+X_s}\lambda^2 + \frac{2\xi[2+(\xi+2)X_s - \xi(\kappa_1+1)X_s^2]}{1+X_s}\lambda + \frac{4\xi^2[\kappa_1+1+2X_s]}{1+X_s} = 0. \tag{27}$$

Using this equation, the following conditions are easily verified:

$$\lim_{\lambda \to -\infty} \det[\lambda \boldsymbol{I} - J(X)] \to -\infty \tag{28}$$

and

$$\det[-J(X)] > 0. \tag{29}$$

Hence, there exists at least one $\lambda \in (\infty, 0)$ such that $\det[\lambda \boldsymbol{I} - J(X)] = 0$, i.e., the system has at least one negative real eigenvalue. Also, numerical calculations of eigenvalues for the practical range of parameters $0 < \kappa_0 < 100$, $0 < \kappa_1 < 10$, and $0.01 < \xi < 10$ reveal that the other two eigenvalues are a complex conjugate pair which have either a positive or negative real part depending upon values of κ_0 and κ_1. In particular the following observations are made.

1) For small values of κ_0, the pair of complex eigenvalues have a negative real part.
2) As κ_0 increases, the real part of the complex eigenvalues gets less negative, and at a critical value of κ_0, the real part changes from negative to positive. Table I shows a typical scenario of the variation of the eigenvalues. The locus is plotted in Fig. 2 for ease of reference.
3) The critical value of κ_0 depends on the values of κ_1 and ξ. Fig. 3 shows the boundary curves where the sign of the real part of the complex eigenvalues changes. On these curves, the system loses stability via a *supercritical Hopf Bifurcation* [11]–[13].

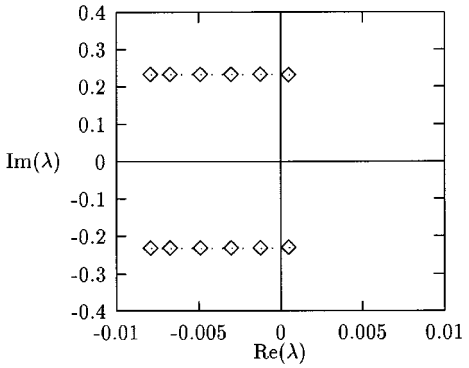

Fig. 2. Locus of the complex eigenvalue pair corresponding to Table I.

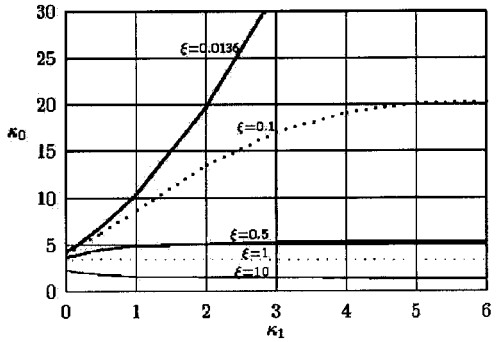

Fig. 3. Boundary of stability. Area below the curve corresponds to stable equilibrium points and that above to unstable equilibrium points.

Remarks: To establish a supercritical Hopf bifurcation formally, one needs to show that, for given ξ and κ_1, there exists κ_0 for which the following conditions are satisfied by the complex eigenvalue pair [13]:

$$\mathrm{Re}(\lambda)\big|_{\kappa_0=\kappa_{0c}} = 0 \tag{30}$$

$$\mathrm{Im}(\lambda)\big|_{\kappa_0=\kappa_{0c}} \neq 0 \tag{31}$$

$$\frac{d}{d\kappa_0}\mathrm{Re}(\lambda)\bigg|_{\kappa_0=\kappa_{0c}} \neq 0 \tag{32}$$

where κ_{0c} is the critical value of κ_0 at which a supercritical Hopf bifurcation occurs. Note that the last condition is necessary to ensure that the complex eigenvalue pair moves from the left side to the right side of the complex plane (preventing it from "locusing" along the imaginary axis). In fact, all the above conditions can be numerically established using (27).

IV. LOCAL TRAJECTORIES FROM DESCRIBING EQUATION

In this section we re-examine the stability in terms of the local trajectories near the equilibrium point. It should be stressed that

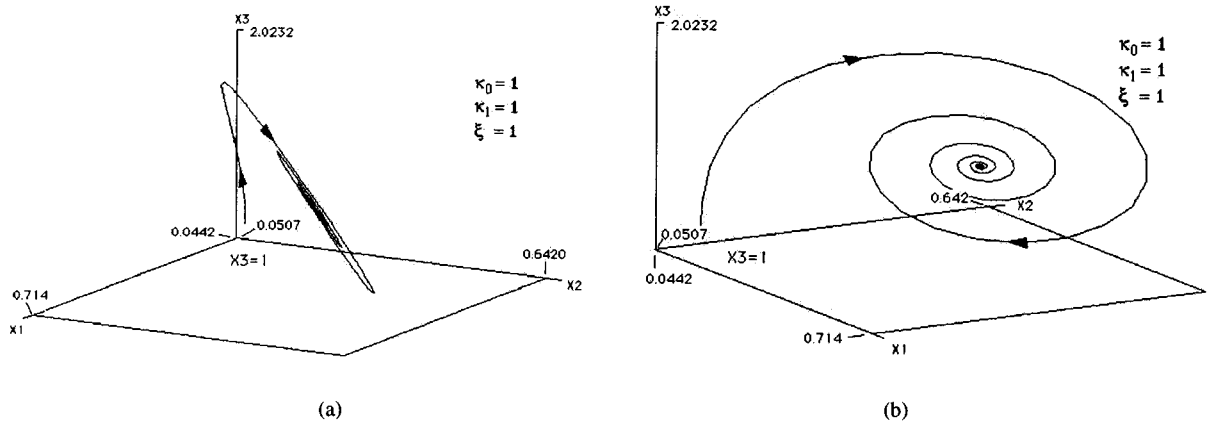

Fig. 4. Two views of the "stable" local trajectory for $\xi = \kappa_0 = \kappa_1 = 1$ (based on averaged model).

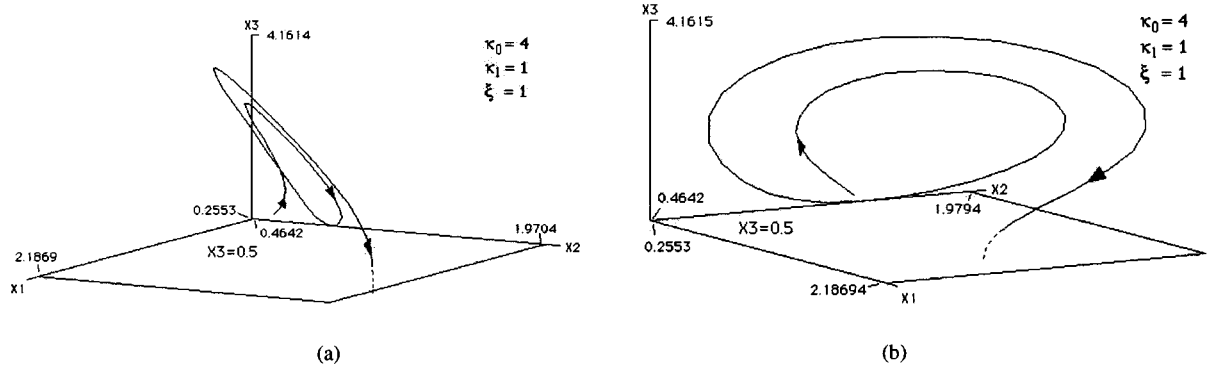

Fig. 5. Two views of the "unstable" local trajectory for $\xi = \kappa_1 = 1, \kappa_0 = 4$ (based on averaged model).

since the use of an averaged model for predicting nonlinear phenomena will become inadequate when stability is lost, our aim in this section is to observe, by plotting the local trajectories, the behavior of the system as it goes from a stable region to an unstable region. For further investigation beyond the bifurcation point, we will resort to the exact piecewise switched model, as will be reported in Section V.

The trajectory of the system near the equilibrium point can be easily derived from the corresponding eigenvalues and eigenvectors. Suppose the eigenvalues and corresponding eigenvectors are

$$\lambda_r,\ \sigma \pm j\omega \quad \text{and} \quad \overline{v}_r,\ \overline{v}_1 \pm j\overline{v}_2. \tag{33}$$

The solution in general is given by

$$\boldsymbol{x}(t) = c_r e^{\lambda_r t}\overline{v}_r + 2c_c e^{\sigma t}[\cos(\omega t + \phi_c)\overline{v}_1 - \sin(\omega t + \phi_c)\overline{v}_2] \tag{34}$$

where c_r, c_c, and ϕ_c are determined by initial conditions. The geometry of the trajectory is best described in terms of the eigenline L_r which is parallel $\overline{v}_r$, and the eigenplane E_c which is spanned by $\overline{v}_1$ and $\overline{v}_2$, the intersection of L_r and E_c being the equilibrium point. Essentially, since the real eigenvalue is negative, the system moves initially in the direction of L_r going toward E_c. At the same time it moves in a helical motion converging toward or diverging away from L_r, depending upon the sign of the real part of the complex eigenvalues. As it lands on E_c, it keeps spiraling along E_c toward or away from the equilibrium point. The following examples illustrate two typical local trajectories, corresponding to a stable and an unstable equilibrium point.

We first examine the stable system with $\xi = \kappa_0 = \kappa_1 = 1$. The Jacobian matrix evaluated at the equilibrium point is

$$J(X) = \begin{pmatrix} -1 & 0 & 1 \\ 2 & -2 & 0 \\ -1.585\,79 & -2.242\,64 & -0.171\,573 \end{pmatrix}. \tag{35}$$

The eigenvalues, λ, and their corresponding eigenvectors, $\overline{v}$, are found as

$$\lambda = -2.740\,51,\ -0.215\,533 \pm j1.694\,91$$
$$\overline{v} = \begin{pmatrix} -0.297\,167 \\ 0.802\,604 \\ 0.517\,222 \end{pmatrix}, \quad \begin{pmatrix} 0.185\,114 \mp j0.399\,955 \\ -0.114\,761 \mp j0.339\,261 \\ 0.823\,104 \end{pmatrix}.$$

Using the INSITE program [14], we can view the trajectory from different perspectives, two of which are shown in Fig. 4.

We next examine the unstable system with $\xi = \kappa_1 = 1$ and $\kappa_0 = 4$. As shown in Fig. 3, the system just loses stability. The Jacobian matrix evaluated at the equilibrium point is

$$J(X) = \begin{pmatrix} -1 & 0 & 1 \\ 2 & -2 & 0 \\ -0.763\,932 & -3.366\,56 & 0.130\,495 \end{pmatrix}. \tag{36}$$

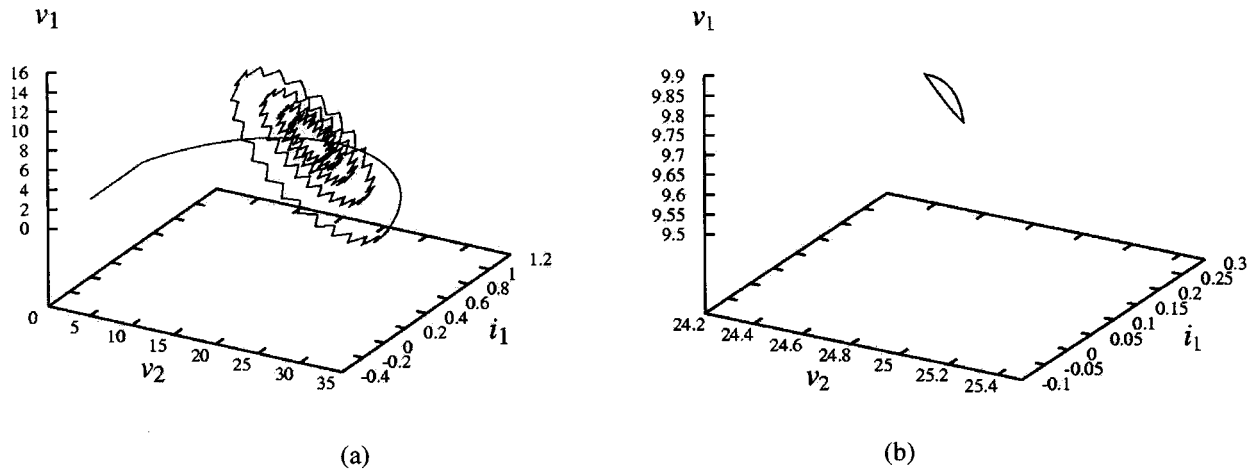

Fig. 6. (a) Trajectory spiralling into stable period-1 orbit and (b) stable period-1 orbit enlarged ($K = 0.4$).

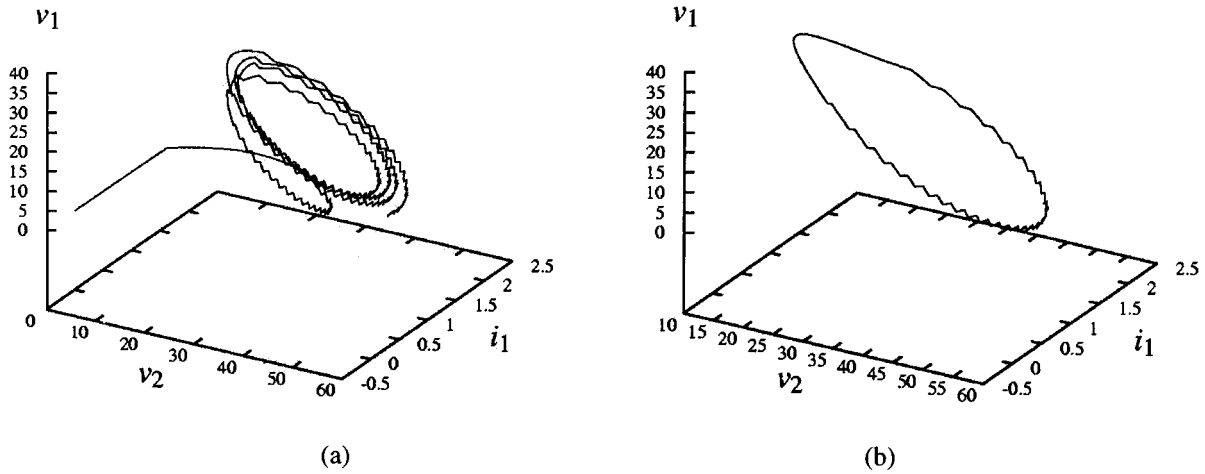

Fig. 7. (a) Trajectory spiralling away from the unstable period-1 orbit and (b) limit cycle ($K = 1.5$).

The eigenvalues, λ, and their corresponding eigenvectors, $\overline{v}$, are found as

$$\lambda = -2.9757,\ 0.053\,096\,5 \pm j1.638\,79$$
$$\overline{v} = \begin{pmatrix} -0.331\,404 \\ 0.679\,316 \\ 0.654\,753 \end{pmatrix}, \begin{pmatrix} 0.233\,197 \mp j0.362\,892 \\ -0.033\,598 \mp j0.326\,689 \\ 0.840\,282 \end{pmatrix}.$$

Using the INSITE program [14] again, we can view the local trajectory from different perspectives, two of which are shown in Fig. 5.

From the above examples, we clearly observe that the system loses stability via Hopf bifurcation as a stable spiral develops into an unstable spiral in the locality of the equilibrium point. In Section V we re-examine the system using cycle-by-cycle computer simulations of the actual switching circuit. As we will see, the system develops into a limit cycle as it loses stability, and further develops into quasi-periodic and chaotic orbits.

V. Computer Simulation Study

Since the foregoing analysis is based on a nonlinear state equation which is derived from an approximate (average) continuous model, it falls short of predicting the details of the bifurcation sequence. Instead of refining the model, we will examine the system using computer simulation which employs an exact piecewise-switched model. Essentially the computer simulation program generates the cycle-by-cycle waveforms of all capacitor voltages and inductor currents by toggling between a set of linear differential equations that describe the constituent linear circuits for all possible switch states. The program also incorporates the free-running current-control algorithm for determining the switch state during simulation.

In our simulation study of the free-running Ćuk converter, we set the input voltage at 15 V and the values of the components as follows:

$$L_1 = L_2 = 0.01\ \text{H}$$
$$C_1 = C_2 = 47\ \mu\text{F}$$
$$R = 40\ \Omega.$$

Note that since we are simulating the actual circuit, the parameters used will be μ and K instead of the dimensionless ones used for analysis. In particular we will focus on the qualitative change of dynamics as the parameters are varied, as hinted from the result of Section III.

To see the trend, it suffices to keep μ constant at 0.01 and vary K. A summary of the observed behavior is as follows. A complete view of the effect of ξ, μ, and K on stability of the

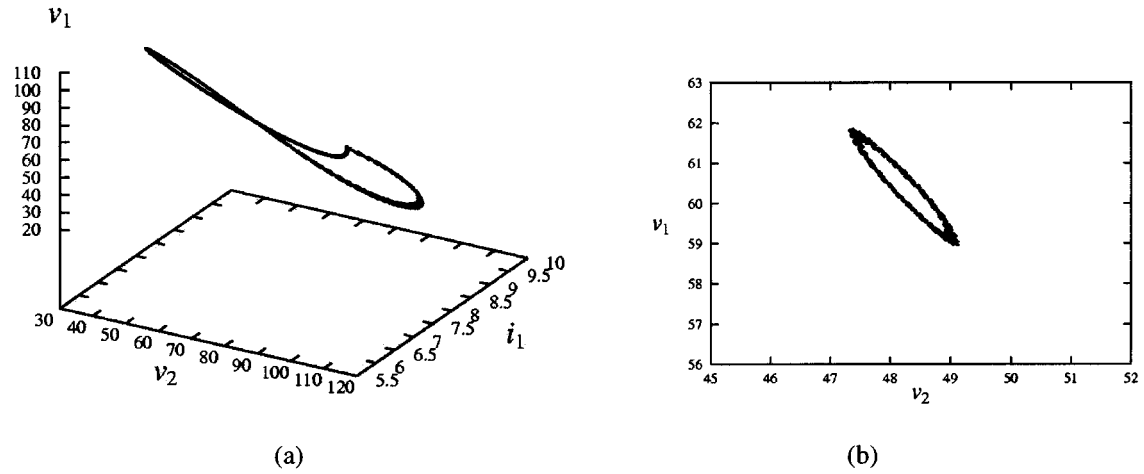

Fig. 8. (a) quasi-periodic orbit and (b) blow-up of a Poincaré section taken at $i_1 = 8.2$ ($K = 10.5$).

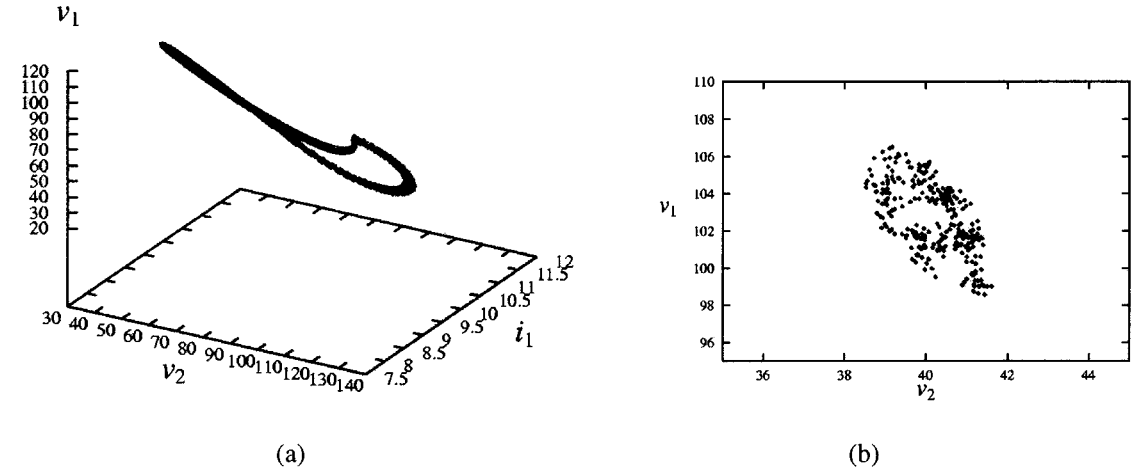

Fig. 9. (a) Chaotic orbit and (b) blow-up of a Poincaré section taken at $i_1 = 9.5$ ($K = 13$).

fundamental equilibrium state will be provided later in this section.

1) When K is small, the trajectory spirals into a fixed period-1 orbit, corresponding to a fixed point in the averaged system. Fig. 6 shows the simulated trajectory and the stable period-1 orbit.
2) For a larger K, the period-1 orbit becomes unstable, and the trajectory spirals outward as shown in Fig. 7(a), and settles into a limit cycle as shown in Fig. 7(b).
3) For yet a larger K, a quasi-periodic orbit can be observed, as shown in Fig. 8(a). A Poincaré section is shown in Fig. 8(b) which is essentially the points of intersection of the trajectory and the vertical plane $i_1 = 8.2$.
4) Finally, chaos occurs when K is further increased. Fig. 9(a) and (b) shows the measured trajectory and a Poincaré section.

Furthermore, based on a number of simulation runs, we can obtain the boundary of stability similar to Fig. 3, for different values of ξ. More precisely, the boundary curves define the values of parameters for which a trajectory changes its qualitative behavior from one that spirals into a fixed period-1 orbit (i.e., fixed point corresponding to the case of averaged model) to one that spirals away from it. As shown in Fig. 10, the stability boundary curves obtained from cycle-by-cycle circuit simulations agree with those of Fig. 3 obtained from the averaged model.

VI. Experimental Verification

We have constructed an experimental circuit for verifying the transition from stable equilibrium states (fixed points), through limit cycles and quasi-periodic orbits, to chaotic attractors. The circuit is shown in Fig. 11(a).

The variation of μ and K is made by adjusting R_μ and R_K in the circuit. To maintain conciseness in this paper, we exemplify in Fig. 12(a)–(d), the qualitative change of the behavior of the system as K is increased. Specifically, the system goes from stable operation to chaotic operation, via limit cycles and quasi-periodic orbits.

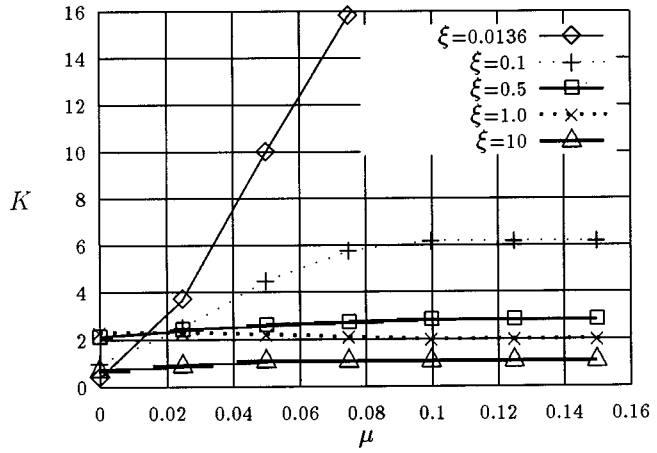

Fig. 10. Boundary of stability from cycle-by-cycle simulation. Area below the curve corresponds to stable fundamental operation and that above to operations other than stable fundamental operation. These curves agree with Fig. 3.

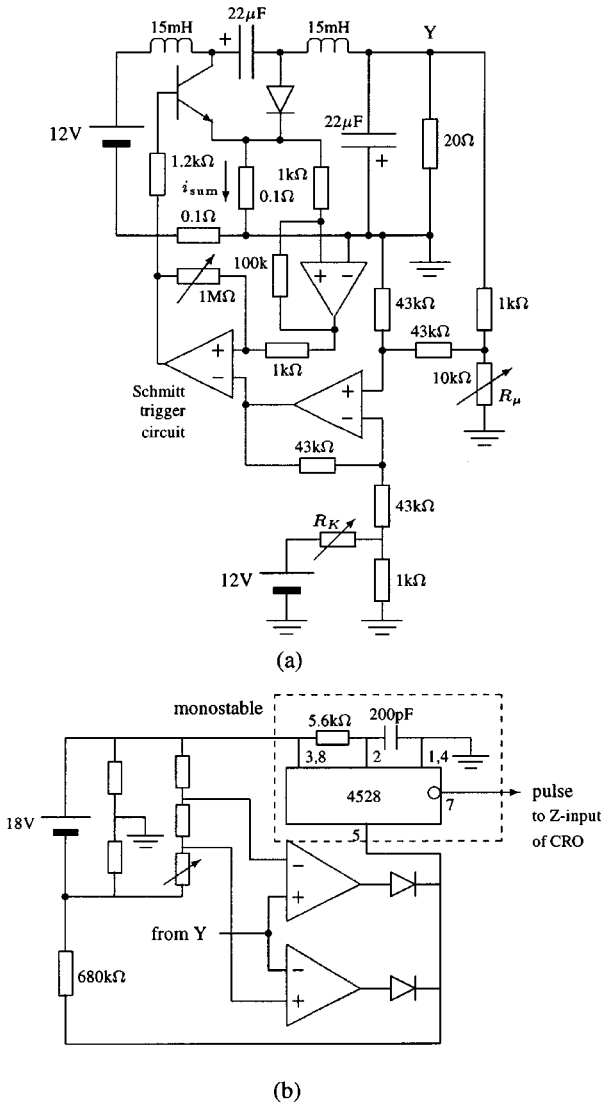

Fig. 11. (a) Experimental free-running Ćuk converter circuit and (b) circuit for highlighting Poincaré section. The x-input of CRO is taken from voltage across the $0.1\ \Omega$ that senses the input inductor current using a differential probe. The y-input of the CRO is taken from output voltage at terminal Y.

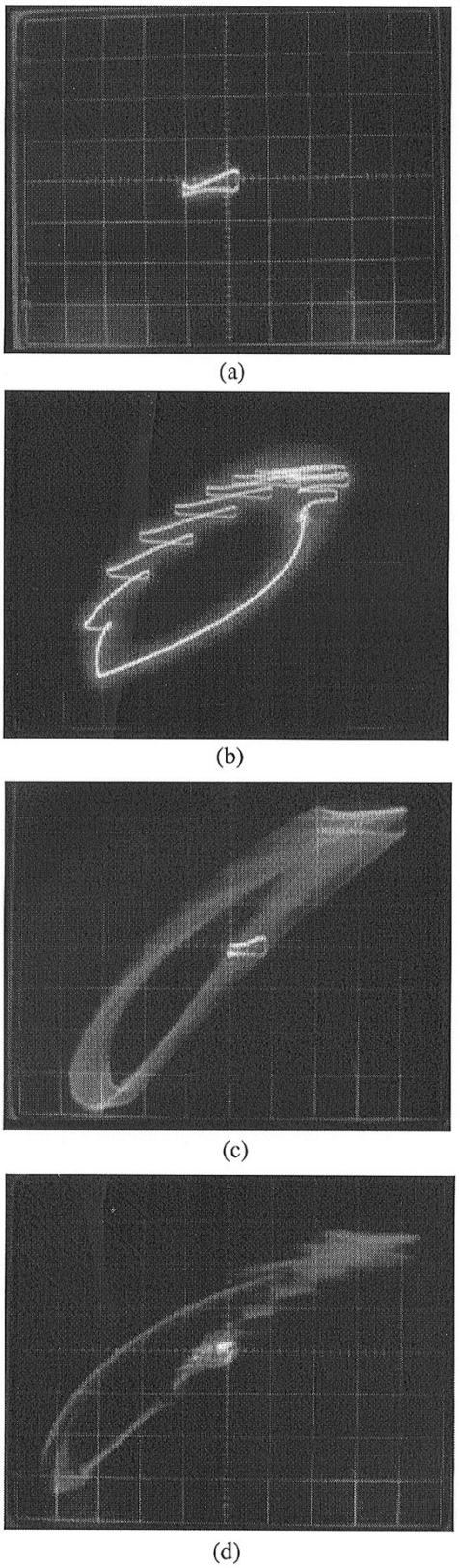

Fig. 12. Phase portraits from autonomous Ćuk converter showing (a) stable period-1 orbit (equilibrium state), (b) limit cycle, (c) quasi-periodic orbit, and (d) chaotic orbit. Poincaré section highlighted in (b)–(d). (Horizontal scale: 0.5 V/div, vertical scale: 0.2 V/div.)

In showing the quasi-periodic orbit and chaotic orbit, we highlight a Poincaré section on the CRO by using a simple

circuit that compares the value of the y-input with a preset value and generates a pulse to the z-input of the CRO whenever the y-input is equal to the preset value. This simple compare circuit is shown in Fig. 11(b). The CRO trace will momentarily brightens when the CRO's z–input receives a pulse. Thus, the CRO is able to highlight a Poincaré section on top of the attractor being displayed.

For the quasi-periodic orbit, we clearly see that the Poincaré section resembles a closed loop around the rim of the torus, whereas for the chaotic orbit, the Poincaré section contains some scattered points.

VII. Conclusion

The Ćuk converter studied in this paper is a very popular design choice for dc/dc converters, but its nonlinear dynamics is seldom seriously analyzed. Previous (probably the only known) attempts in studying the nonlinear dynamics of this converter have focused on fixed-frequency current-mode control [15], [16] which permits a describing discrete-time iterative map to be used for analysis. In this paper we extend the study to a different mode of control which is based on a free-running or self-oscillating loop.

Due to their simplicity, free-running switching converters are commonly used in the construction of low-cost power supplies. For simple free-running buck, boost, and buck-boost types of converters, only fixed points and limit cycles are possible. However, for higher-order free-running converters, such as those employing the Ćuk, SEPIC, and Zeta converters, quasi-periodicity and chaos are possible. In this paper, we examine in particular the nonlinear behavior of a free-running Ćuk converter. Analysis of the describing autonomous equations reveals that the system loses stability via a Hopf bifurcation. Our study has been carried out in three phases. We first employ an analytical model to predict possible onsets of Hopf bifurcation by studying the movement of the complex eigenvalues of system's Jacobian at the equilibrium point as some chosen parameters are changed. In particular, we have observed the way the system loses stability using the INSITE software, which can be used to generate trajectories for any given dynamical system. Our second phase of study has been resorted to computer simulations of the actual system using an exact piecewise-switched model. The bifurcation from a stable equilibrium state, through limit cycles and quasi-periodic orbits, to chaos has been observed. Finally, we have confirmed the predicted Hopf bifurcation and the simulated sequence of changes in qualitative behavior by experimental measurements of the actual circuit.

Acknowledgment

The authors wish to thank the reviewers for their thorough review of this paper and for helpful suggestions and comments. The efforts of P. Li and H. L. Chan in performing the experiments are gratefully acknowledged.

References

[1] D. C. Hamill, "Power electronics: A field rich in nonlinear dynamics," in *Proc. Int. Spec. Workshop Nonlinear Dynamics of Electron. Syst.*, Dublin, Ireland, 1995, pp. 165–178.
[2] C. K. Tse, "Flip bifurcation and chaos in three-state boost switching regulators," *IEEE Trans. Circuits Syst.—Part I*, vol. 41, pp. 16–23, Jan. 1994.
[3] ——, "Chaos from a buck switching regulator operating in discontinuous mode," *Int. J. Circ. Theory Appl.*, vol. 22, no. 4, pp. 263–278, July 1994.
[4] D. C. Hamill, J. H. B. Deane, and D. J. Jefferies, "Modeling of chaotic dc/dc converters by iterative nonlinear mappings," *IEEE Trans. Power Electron.*, vol. 7, pp. 25–36, Jan. 1992.
[5] E. Fossas and G. Olivar, "Study of chaos in the buck converter," *IEEE Trans. Circuits Syst.—Part I*, vol. 43, pp. 13–25, Jan. 1996.
[6] M. di Bernardo, L. Glielmo, F. Garofalo, and F. Vasca, "Switching, bifurcations and chaos in dc/dc converters," *IEEE Trans. Circuits Syst.—Part I*, vol. 45, pp. 133–141, Feb. 1998.
[7] S. Jalali, I. Dobson, R. H. Lasseter, and G. Venkataramanan, "Switching time bifurcations in a thyristor controlled reactor," *IEEE Trans. Circuits Syst.—Part I*, vol. 43, pp. 209–218, Mar. 1996.
[8] K. Chakrabarty, G. Podder, and S. Banerjee, "Bifurcation behavior of buck converter," *IEEE Trans. Power Electron.*, vol. 11, pp. 439–447, May 1995.
[9] R. Redl, "Small-signal high-frequency analysis of the free-running current-mode-controlled converter," in *IEEE Power Electronics Specialists Conf.*, 1991, pp. 897–906.
[10] S. C. Wong and Y. S. Lee, "SPICE modeling and simulation of hysteretic current-controlled Ćuk converter," *IEEE Trans. Power Electron.*, vol. 8, pp. 580–587, Oct. 1993.
[11] J. Hale and H. Kocak, *Dynamics and Bifurcations*. New York: Springer-Verlag, 1991.
[12] S. H. Strogatz, *Nonlinear Dynamics and Chaos*. Reading, PA: Addison-Wesley, 1994.
[13] K. T. Alligood, T. D. Sauer, and J. A. Yorke, *Chaos: An Introduction to Dynamical Systems*. New York: Springer-Verlag, 1996.
[14] T. S. Parker and L. O. Chua, *Practical Numerical Algorithms for Chaotic Systems*. New York: Springer-Verlag, 1989.
[15] C. K. Tse and W. C. Y. Chan, "Chaos from a current-programmed Ćuk converter," *Int. J. Circ. Theory Appl.*, vol. 23, pp. 217–225, July 1995.
[16] C. K. Tse, S. C. Fung, and M. W. Kwan, "Experimental confirmation of chaos in a current-programmed Ćuk converter," *IEEE Trans. Circuits Syst.—Part I*, vol. 43, July 1996.

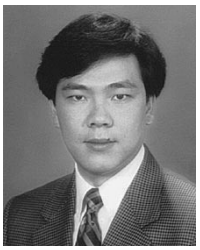

C. K. Tse (M'90–SM'97) received the B.Eng. (Hons) degree with first class honors in electrical engineering and the Ph.D. degree from the University of Melbourne, Australia, in 1987 and 1991, respectively.

He is currently an Associate Professor with Hong Kong Polytechnic University, Hong Kong, and his research interests include chaotic dynamics and power electronics. He has worked in software design with an Australian database development company and spent a short period of time with ASTEC Power Modules, Hong Kong, as a Senior Engineer. He is the author of *Linear Circuit Analysis* (London, U.K.: Addison-Wesley 1998), and coholder of a US patent.

He serves currently as an Associate Editor for both IEEE Transactions on Circuits and Systems—Part I: Fundamental Theory and Applications and IEEE Transactions on Power Electronics. In 1987, Dr. Tse was awarded the L. R. East Prize by the Institution of Engineers, Australia. In 1997, he received the President's Award for Achievements in Research and the Best Teacher Award from Hong Kong Polytechnic University.

Y. M. Lai (M'92) received the B.Eng. (Hons) and M.Eng.Sc. degrees in electrical engineering, respectively, from the University of Western Australia, Australia, in 1983, and the University of Sydney, Australia, in 1986. He obtained the Ph.D. degree from Brunel University, U.K., in 1997.

He is currently an Assistant Professor with Hong Kong Polytechnic University, Hong Kong, and his research interests include computer-aided design of power electronics and nonlinear dynamics. Prior to joining the University, he held technical positions with National Semiconductors, Derek Philips Associates, and Siliconix Hong Kong Limited.

Dr. Lai is a member of the Institution of Engineers, Australia, and is a Chartered Professional Engineer in Australia.

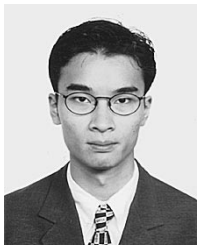

H. H. C. Iu (S'98) received the B.Eng. (Hons) degree in electrical and electronic engineering from the University of Hong Kong, Hong Kong, in 1997. He is currently working toward the Ph.D. degree at Hong Kong Polytechnic University, Hong Kong, in the areas of identification, nonlinear analysis, bifurcation phenomena, and chaotic dynamics of power electronics circuits.